Real-space variational Gutzwiller wave functions for the Anderson-Hubbard model

A. Farhoodfar,[1,*] X. Chen,[1] R. J. Gooding,[1] and W. A. Atkinson[2]
[1]*Department of Physics, Queen's University, Kingston, Ontario, Canada K7L 3N6*
[2]*Department of Physics, Trent University, Peterborough, Ontario, Canada K9J 7B8*
(Received 19 March 2009; revised manuscript received 10 June 2009; published 13 July 2009)

Partially projected Gutzwiller variational wave functions are used to describe the ground state of disordered interacting systems of fermions. We compare several different variational ground states with the exact ground state for disordered one-dimensional chains, with the goal of determining a minimal set of variational parameters required to accurately describe the spatially inhomogeneous charge densities and spin correlations. We find that, for weak and intermediate disorder, it is sufficient to include spatial variations of the charge densities in the product state alone provided that screening of the disorder potential is accounted for. For strong disorder, this prescription is insufficient and it is necessary to include spatially inhomogeneous variational parameters as well.

DOI: 10.1103/PhysRevB.80.045108 PACS number(s): 71.10.Fd, 71.23.An, 71.27.+a

I. INTRODUCTION

The problem of how to treat theoretically systems of interacting electrons in disordered materials extends over many decades. The most difficult problems to solve are ones in which the physical properties of interest depend on spatial correlations of individual realizations of the disorder potential. In this case, the majority of disorder-averaged approximations fail and more sophisticated analytical or numerical techniques are required. Anderson localization and Coulomb gap physics are two examples of such problems.[1] The problems are particularly challenging in narrow-band materials where conventional approximations for the Coulomb interaction are poor.[2]

There has been particular interest in low-dimensional disordered systems in recent years. For example, many transition-metal oxides, especially the quasi-two-dimensional high-temperature superconductors,[3–10] are intrinsically disordered by chemical doping and have electronic properties that appear to be strongly susceptible to disorder. More recently, experiments have demonstrated the formation of a two-dimensional electron gas at the interface of an otherwise insulating La_2CuO_4/Sr_2TiO_4 heterostructure[11–14] and there are indications that the electronic states at the interface are strongly influenced by inhomogeneities.[15] A more fundamental question that has arisen in the past decade is whether interactions may drive a delocalization transition in thin metal films.[16]

Theoretically, we can investigate the relation between disorder and electron-electron interactions by studying the Anderson-Hubbard (AH) Hamiltonian. The AH model is the Hubbard model[17] for a lattice with site energies chosen from a random distribution

$$\mathcal{H} = \sum_{i,\sigma} V_i \hat{n}_{i,\sigma} - t \sum_{\langle i,j\rangle,\sigma} c^{\dagger}_{i,\sigma} c_{j,\sigma} + U \sum_{i} \hat{n}_{i,\uparrow}\hat{n}_{i,\downarrow}, \tag{1}$$

where $i,j=1,\ldots,N$ denote the sites of the lattice, $\langle i,j\rangle$ implies that i and j are nearest neighbors, $c_{i,\sigma}(\hat{n}_{i,\sigma})$ is the destruction (number) operator for an electron at site i with spin σ, and the hopping energy is denoted by $-t$. The on-site energy at site i is given by V_i and U is the electron repulsion of two electrons sharing the same site.

The only known exact solution for the AH Hamiltonian is in infinite dimensions[18] and we thus have to use approximate methods in finite dimensions. The various approximate methods used previously include self-consistent Hartree-Fock theory,[19–23] dynamical mean-field theories,[24–31] and exact numerical calculations for small clusters.[20,32–34] Of particular relevance to the current work is a recent variational wave-function approach by Pezzoli *et al.*,[35] which we discuss below.

Here, we consider a variational wave-function approach based on a modification of the Gutzwiller wave function (GWF) (Refs. 36–38) to include spatial inhomogeneity. The GWF is the simplest variational wave function for Hubbard-type Hamiltonians and is given by

$$|\Psi_{\mathrm{GWF}}\rangle = \prod_i [1-(1-g)\hat{n}_{i\uparrow}\hat{n}_{i\downarrow}]|\psi_{\mathrm{ps}}\rangle, \tag{2}$$

where $|\psi_{\mathrm{ps}}\rangle$ is a reference product (i.e., Slater-determinant) state. This function was originally introduced to study the correlations of the ground state of the Hubbard Hamiltonian. The variational parameter $0\leq g\leq 1$ incorporates the effect of the Hubbard repulsion between electrons of opposite spins on the same site and is obtained by minimizing the energy functional

$$E_{\mathrm{GWF}} = \frac{\langle\Psi_{\mathrm{GWF}}|\mathcal{H}|\Psi_{\mathrm{GWF}}\rangle}{\langle\Psi_{\mathrm{GWF}}|\Psi_{\mathrm{GWF}}\rangle}. \tag{3}$$

We note that $g=1$ corresponds to an unprojected wave function, while $g=0$ corresponds to a fully projected wave function in which there are no doubly occupied sites. Physically, the $g=0$ projection captures an essential feature of the large-U Hubbard model: it generates local paramagnetic moments without breaking the spin-rotational invariance of the lattice.

The GWF is hard to treat analytically, even for the disorder-free Hubbard Hamiltonian where analytical results have only been obtained in one[39–42] and infinite[43] dimensions. The variational GWF is therefore primarily a numeri-

cal method.[38,44–46] Our goal is to investigate the quality of a number of simple variational wave functions by comparison of the variational ground states with exact diagonalization calculations on small clusters.

The GWF has certain well-known limitations:[38] it fails in the disorder-free case, for example, to describe the Mott transition at half-filling in finite dimensions. In general, the GWF can be improved by the addition of nonlocal Jastrow factors that describe the long-range interactions between charge-density excitations.[47,48] Recently, Pezzoli *et al.*[35] used variational methods to study the AH Hamiltonian in two dimensions. Their particular focus was on states near the Mott transition, which necessitated the inclusion of the Jastrow factors. Furthermore, they included spatial inhomogeneity in both the product state $|\psi_{\rm ps}\rangle$ and in their local variational factors (e.g., $g \to g_i$). These extra degrees of freedom resulted in a large number of variational parameters (several hundred for a typical lattice) and required sophisticated minimization schemes for the energy functional.[49] It is therefore worth asking under what circumstances we can safely reduce the number of variational parameters and still obtain reasonable results for the variational wave function.

In the current work, we examine trial wave functions with a small number of variational parameters. Spatial inhomogeneity is incorporated in the product state wave functions $|\psi_{\rm ps}\rangle$, however, the variational parameters are taken to be spatially homogeneous. Our main result is that for weak and intermediate disorder, this simple wave function gives a surprisingly good description of the ground state away from the Mott transition. It is only for strong disorder that our simple ansatz for $|\Psi_{\rm GWF}\rangle$ breaks down.

The paper is organized as follows. In Sec. II, we describe the variational wave function in detail and introduce a number of candidate states for $|\psi_{\rm ps}\rangle$. In Sec. III, we assess the quality of the different trial wave functions by comparing with both exact diagonalization and unrestricted Hartree-Fock (UHF) calculations. The latter comparison is motivated by the fact that UHF has been, until recently, the standard numerical technique for studying disordered systems. Furthermore, a recent work[20] has suggested that UHF actually provides good quantitative results for some local physical quantities in disordered systems (namely, that disorder improves the quality of the UHF approximation). We discuss the strengths and limitations of the simple GWF in Sec. IV and conclusions are given in Sec. V.

II. METHOD: GUTZWILLER VARIATIONAL APPROACH

In this section, we introduce a number of variational states $|\Psi_{\rm GWF}\rangle$ that will be used for calculations. We want to keep the simple form of the projection operator in Eq. (2), which means that spatial inhomogeneity is introduced entirely through the product state. It is for this reason that we consider a variety of product states, with the goal of determining how large an effect the initial choice for $|\psi_{\rm ps}\rangle$ makes on the final $|\Psi_{\rm GWF}\rangle$.

A. Product states

Assume that we are seeking the N_e-electron variational ground state for an N-site lattice with a particular realization of the disorder potential. We then take $|\psi_{\rm ps}\rangle$ to be the N_e-electron ground state of an N-site bilinear (effectively noninteracting) Hamiltonian $\mathcal{H}_{\rm bl}$ whose disorder potential is determined by the site energies of $\mathcal{H}$. We examine three possibilities: (i) $\mathcal{H}_{\rm bl}$ is the Anderson Hamiltonian, obtained by setting $U=0$ in Eq. (1) and renormalizing the site energies with a variational screening parameter, (ii) $\mathcal{H}_{\rm bl}$ is the self-consistent Hartree-Fock (HF) decomposition of $\mathcal{H}$, and (iii) $\mathcal{H}_{\rm bl}$ is the HF decomposition of $\mathcal{H}$ with screened site energies.

Since $\mathcal{H}_{\rm bl}$ is bilinear, $|\psi_{\rm ps}\rangle$ can be represented by

$$|\psi_{\rm ps}\rangle = \gamma_1^\dagger \gamma_2^\dagger \gamma_3^\dagger \ldots \gamma_{N_e}^\dagger |0\rangle = \prod_{\alpha=1}^{N_e} \gamma_\alpha^\dagger |0\rangle, \tag{4}$$

where α labels the lowest-energy single-particle eigenstates of $\mathcal{H}_{\rm bl}$, ordered from lowest ($\alpha=1$) to highest ($\alpha=N_e$) energy, and $\gamma_\alpha^\dagger$'s are creation operators for these eigenstates. The $\gamma_\alpha^\dagger$'s can be related to the real-space creation operators, $c_I^\dagger$, by

$$\gamma_\alpha^\dagger = \sum_{I=1}^{2N} G_{I,\alpha} c_I^\dagger, \tag{5}$$

where $G_{I,\alpha}$ are the elements of the unitary matrix $\underline{\underline{G}}$ that diagonalizes $\mathcal{H}_{\rm bl}$, I labels the spin and site with $1 \le I \le 2N$. Then we have

$$|\psi_{\rm ps}\rangle = \sum_{I_1,\ldots,I_{N_e}=1}^{2N} G_{I_1,1} \ldots G_{I_{N_e},N_e} c_{I_1}^\dagger \ldots c_{I_{N_e}}^\dagger |0\rangle, \tag{6}$$

which can be rewritten, using the anticommutation relations of the creation operators, as

$$|\psi_{\rm ps}\rangle = \sum_{I_1<\cdots<I_{N_e}} D[\underline{\underline{G}}(\underline{I})] c_{I_1}^\dagger \ldots c_{I_{N_e}}^\dagger |0\rangle, \tag{7}$$

where $D[\underline{\underline{G}}(\underline{I})]$ is a Slater determinant

$$D[\underline{\underline{G}}(\underline{I})] \equiv \det \begin{pmatrix} G_{I_1,1} & \cdots & G_{I_1,N_e} \\ G_{I_2,1} & \cdots & G_{I_2,N_e} \\ \cdots & \cdots & \cdots \\ \cdots & \cdots & \cdots \\ G_{I_{N_e},1} & \cdots & G_{I_{N_e},N_e} \end{pmatrix}. \tag{8}$$

The vector $\underline{I}=(I_1,\ldots,I_{N_e})$ labels different configurations of the electrons. For a given $\underline{I}$, $D[\underline{\underline{G}}(\underline{I})]$ gives the weight of that configuration of electrons in the product state. Using Eq. (2), we can write

$$|\Psi_{\rm GWF}\rangle = \sum_{I_1<\cdots<I_{N_e}} D[\underline{\underline{G}}(\underline{I})] \prod_{i=1}^{N} [1-(1-g)\hat{n}_{i\uparrow}\hat{n}_{i\downarrow}] c_{I_1}^\dagger \ldots c_{I_{N_e}}^\dagger |0\rangle. \tag{9}$$

In general, $|\Psi_{\rm GWF}\rangle$ contains a large number of terms and must be calculated approximately, for example, using variational Monte Carlo methods. In the current work, we restrict ourselves to small clusters where $|\Psi_{\rm GWF}\rangle$ can be evaluated exactly.

TABLE I. Summary of the different bilinear Hamiltonians $\mathcal{H}_{\rm bl}$ used to generate $|\psi_{\rm ps}\rangle$.

	$U\bar{n}_{i\uparrow(\downarrow)}$	V_i'
DFSGW	$U\bar{n}_{i\uparrow(\downarrow)}=0$	$V_i'=V_i/\varepsilon$
PMGW	$U\bar{n}_{i\uparrow}=U\bar{n}_{i\downarrow}$	$V_i'=V_i$
PMGW(g,ε)	$U\bar{n}_{i\uparrow}=U\bar{n}_{i\downarrow}$	$V_i'=V_i/\varepsilon$

Our first choice of $\mathcal{H}_{\rm bl}$ is the noninteracting disordered Hamiltonian where the disorder potential is screened. The on-site energies are reduced,

$$\underbrace{V_i}_{\text{bare disorder potential}} \rightarrow \underbrace{V_i' = \frac{V_i}{\varepsilon}}_{\text{screened disorder potential}},$$

where the screening factor ε is a variational parameter. Both variational parameters ε and g are determined so as to minimize the total GWF energy $E_{\rm GWF}(\varepsilon,g)$. We refer to this variational wave function as the disordered Fermi-sea GWF (DFSGW).

Our remaining choices of $\mathcal{H}_{\rm bl}$ are based on the HF decomposition of $\mathcal{H}$. The four-fermion interaction term in Eq. (1) can be written as

$$\begin{aligned} U\hat{n}_{i\uparrow}\hat{n}_{i\downarrow} &= U(\bar{n}_{i\uparrow}+\delta\hat{n}_{i\uparrow})(\bar{n}_{i\downarrow}+\delta\hat{n}_{i\downarrow}) \\ &\approx U\hat{n}_{i\uparrow}\bar{n}_{i\downarrow}+U\hat{n}_{i\downarrow}\bar{n}_{i\uparrow}-U\bar{n}_{i\uparrow}\bar{n}_{i\downarrow}, \end{aligned} \tag{10}$$

where $\bar{n}_{i\sigma}\equiv\langle\hat{n}_{i\sigma}\rangle$ and $\delta\hat{n}_{i\sigma}=\hat{n}_{i\sigma}-\bar{n}_{i\sigma}$.[50] The HF Hamiltonian, using Eqs. (1) and (10), can be written as

$$\mathcal{H}_{\rm HF}=\mathcal{H}_{\rm bl}-U\sum_{i=1}^{N}\bar{n}_{i\uparrow}\bar{n}_{i\downarrow}, \tag{11}$$

where the second term on the right-hand side is just a constant, and

$$\mathcal{H}_{\rm bl}=\sum_i\sum_\sigma(V_i+U\bar{n}_{i-\sigma})\hat{n}_{i\sigma}-t\sum_{\langle i,j\rangle\sigma}c_{i\sigma}^\dagger c_{j\sigma}, \tag{12}$$

where $\bar{n}_{i\sigma}$ are determined self-consistently.

Our second choice of $\mathcal{H}_{\rm bl}$ is the paramagnetic HF (PMHF) Hamiltonian, i.e., Eq. (12) with $\bar{n}_{i\uparrow}=\bar{n}_{i\downarrow}$. Here g is the only variational parameter and we refer to the variational wave function for this choice as PMGW.

Our third choice of $\mathcal{H}_{\rm bl}$ is the PMHF Hamiltonian with a screened disorder potential. For this case, the on-site energies of Eq. (12) are reduced to $V_i'=V_i/\varepsilon$, and again, both variational parameters ε and g are determined so as to minimize the total GWF energy. These calculations are more computationally demanding than the previous two because $\bar{n}_{i\sigma}$ must be determined self-consistently for each ε. We refer to the variational wave function for this choice as PMGW (g,ε). The different $\mathcal{H}_{\rm bl}$ are summarized in Table I.

As a simple illustration, in the Appendix we compare the different product states for a disordered two-site system. As in the disorder-free case,[48] the sample GWFs span the Hilbert space of a two-site case and yield exact results.

III. RESULTS: COMPARISONS OF EXACT AND VARIATIONAL QUANTITIES

In this section we show results for PMGW, PMGW(g,ε), and DFSGW variational states for small clusters where variational calculations may be compared to exact diagonalization calculations. Motivated by the earlier work[20] demonstrating that the UHF approximation (in which the self-consistently determined $\bar{n}_{i\sigma}$ may depend on σ) provides accurate charge densities in disordered systems, we also consider UHF as a benchmark for the various GWF calculations.

The quantities that we have calculated are as follows:

(i) we have calculated the absolute difference of the exact and the variational energies per site defined by

$$\delta E_{\rm var}\equiv\frac{1}{N}|E^{\rm var}-E^{\rm ex}|. \tag{13}$$

(ii) We have evaluated the magnitude of the overlap between the exact and variational wave functions given by

$$|\langle\Psi_{\rm ex}|\Psi_{\rm var}\rangle|. \tag{14}$$

(iii) We have calculated the local charge densities according to

$$\bar{n}_i\equiv\langle\Psi|\sum_\sigma\hat{n}_{i,\sigma}|\Psi\rangle, \tag{15}$$

where $|\Psi\rangle$ represents the exact or variational wave function.

(iv) We have calculated the local spin correlations for near-neighbor sites in one dimension,

$$\langle\mathbf{S}_i\cdot\mathbf{S}_{i+1}\rangle\equiv\langle\Psi|\mathbf{S}_i\cdot\mathbf{S}_{i+1}|\Psi\rangle. \tag{16}$$

(v) We have calculated the average absolute difference of charge densities given by

$$\langle\delta\bar{n}\rangle\equiv\frac{1}{N}\sum_{i=1}^{N}|\bar{n}_i^{\rm var}-\bar{n}_i^{\rm ex}|. \tag{17}$$

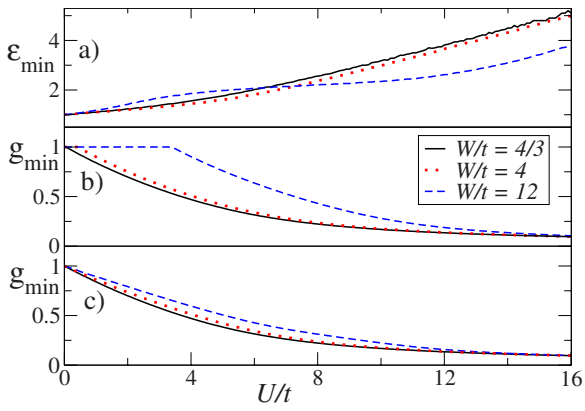

FIG. 1. (Color online) Variational parameters for the DFSGW and PMGW approximations for the six-site cluster for weak $(W/t=4/3)$, intermediate $(W/t=4)$, and strong disorders $(W/t=12)$. The DFSGW (a) screening factor $\varepsilon_{\rm min}$ and (b) projection $g_{\rm min}$ are shown as functions of U. The PMGW projection $g_{\rm min}$ is shown in (c).

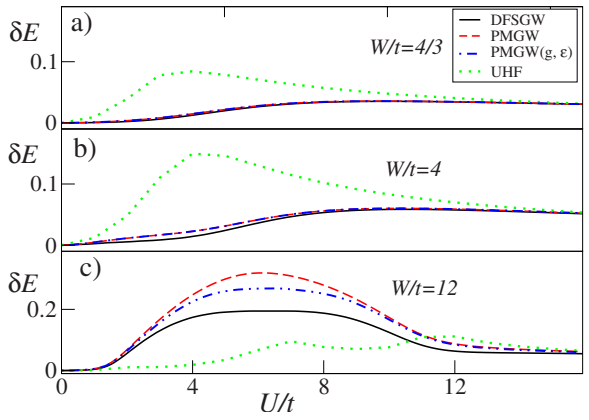

FIG. 2. (Color online) Difference between variational and exact energies for (a) weak, (b) intermediate, and (c) strong disorders. Results are shown for DFSGW, PMGW (g,ε), PMGW, and UHF. The UHF results are shown for step size $\Delta U=t$. Note that for weak and intermediate disorder, the PMGW and PMGW(g,ε) curves coincide.

(vi) We have calculated the average absolute difference of local spin correlations defined by

$$\langle \delta\overline{\mathbf{S}\cdot\mathbf{S}'}\rangle \equiv \frac{1}{N}\sum_{i=1}^{N} |\langle \mathbf{S}_i\cdot\mathbf{S}_{i+1}\rangle^{\mathrm{var}} - \langle \mathbf{S}_i\cdot\mathbf{S}_{i+1}\rangle^{\mathrm{ex}}|. \quad (18)$$

A. Six-site cluster

We have examined several complexions of disorder for the 6×1 cluster with periodic boundary conditions at half-filling ($N_e=6$) and focus on one representative configuration. The disorder potential for the configuration is

$$V_i = 0, -0.18W, +0.5W, +0.12W, -0.5W, +0.3W,$$

where W is the strength of disorder. The bandwidth $D=4t$ for the noninteracting ordered cluster sets the scale for the disorder potential, and we have examined weak $(W/t=4/3)$, intermediate $(W/t=4)$, and strong $(W/t=12)$ disorders. Our results are shown in Figs. 1–7.

We show first, in Fig. 1, the variational parameters $g_{\min}$ and $\varepsilon_{\min}$ that minimize the total energy for the DFSGW and

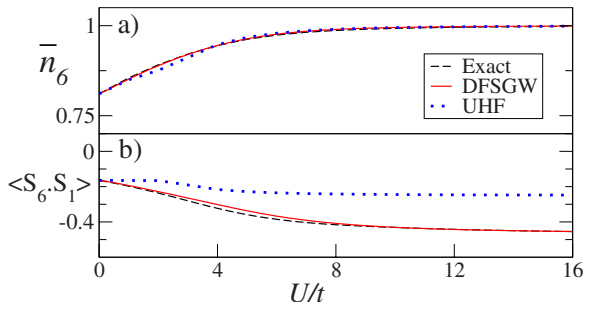

FIG. 3. (Color online) Comparison of (a) the charge density for the sixth site, $\bar{n}_6$ and (b) $\langle \mathbf{S}_6\cdot\mathbf{S}_1\rangle$ for exact results (black dashed lines), DFSGW (solid red lines) and UHF (dotted blue lines). The UHF results are shown for step size $\Delta U=t$. Results are for $W/t=4/3$.

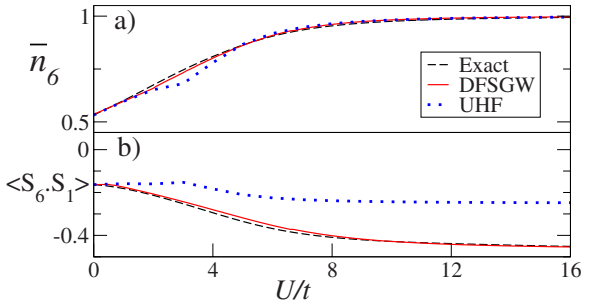

FIG. 4. (Color online) As in Fig. 3, but for $W/t=4$.

PMGW approximations. The PMGW(g,ε) approximation is numerically equivalent to PMGW (i.e., $\varepsilon_{\min}=1$) for weak and intermediate disorder and is therefore not shown.

For the DFSGW approximation, $\varepsilon_{\min}$ is an increasing function of U, indicating that interactions effectively screen the disorder potential, making the charge distribution more homogeneous than in the noninteracting case. At weak and intermediate disorder, $\varepsilon_{\min}$ is only weakly affected by the disorder potential; however, for strong disorder there is a significant reduction in screening. For all W, $\varepsilon_{\min}\propto U$ when $U>W$. For weak disorder, $g_{\min}$ is quantitatively like that of the ordered case,[38] while for strong disorder the wave function is unprojected $(g_{\min}=1)$ for $U<3.4t$. In all cases, the projection is substantial when $U\gg W,D$.

For the PMGW approximation, the screening is implicit in the self-consistency of charge densities in the HF product state. For weak and intermediate disorder, $g_{\min}$ is quantitatively similar to the DFSGW case; however, for strong disorder $g_{\min}<1$ for all nonzero U's in contrast to the DFSGW case. The quantitative similarity between the different $g_{\min}$ curves in Fig. 1(c), unlike Fig. 1(b), suggests that the self-consistent HF solutions screen the disorder potential more completely than the variational parameter $\varepsilon_{\min}$ in the DFSGW approximation.

We now move to a discussion of the quality of the variational solutions. In Fig. 2, we show the differences between the exact and variational energies. For weak and intermediate disorders δE_{GWF} is smaller than δE_{UHF} suggesting that GWFs are better than UHF. Both the DFSGW and PMGW variational states have similar δE [recall that PMGW (g,ε) is numerically equivalent to PMGW here] and detailed comparisons of the variational states (not shown) find little difference in their predictions for the physical observables defined at the beginning of Sec. III.

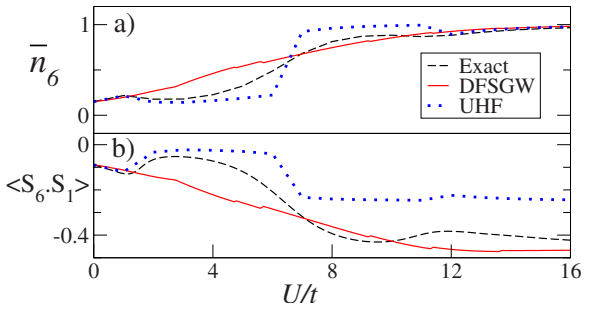

FIG. 5. (Color online) As in Fig. 3, but for $W/t=12$.

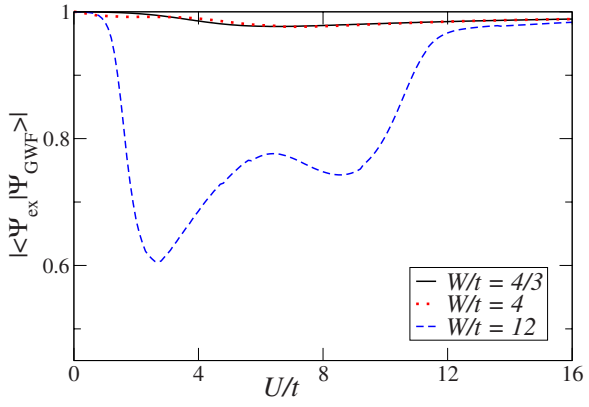

FIG. 6. (Color online) Magnitude of the overlap of the exact and DFSGW wave functions for the six-site disordered cluster.

For strong disorder the situation is a little different: the value for δE_{GWF} is different for the three variational states, with DFSGW having the smallest δE. However, for most values of U, the UHF approximation has a lower energy than any of the GWF approximations.

In Figs. 3–5 we compare charge densities and spin correlations for variational and exact calculations. For clarity, GWF results are shown only for the DFSGW approximation. Furthermore, we show the charge density as a function of U for only one representative site in the cluster and we show the spin correlations for only a single representative pair of sites.

Figure 3 shows the results for weak disorder, $W/t=4/3$. Here, $W \ll D$ and the bandwidth D is therefore the relevant energy scale for the crossover between the weakly and strongly interacting limits as a function of U (similar to the disorder-free case).[38] The figure shows that both the UHF and DFSGW do a good job of reproducing the local charge densities for all U's, but that the DFSGW is significantly better at reproducing the spin correlations. This is particularly true at large U where local moments have formed (i.e., all sites are singly occupied). Within the UHF approximation, local moment formation coincides with the onset of classical static magnetic moments such that $\langle \mathbf{S}_i \cdot \mathbf{S}_{i+1} \rangle \rightarrow -1/4$. In contrast, the DFSGW gives

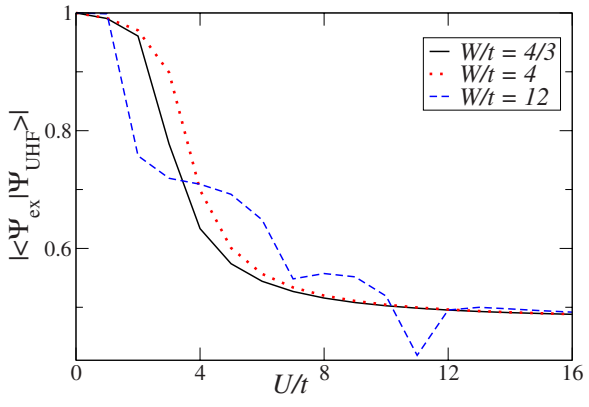

FIG. 7. (Color online) Magnitude of the overlap of the exact and UHF wave functions for the six-site disordered cluster. Data are shown for step size $\Delta U=t$.

$\langle \mathbf{S}_i \cdot \mathbf{S}_{i+1} \rangle \rightarrow -0.45$ for large U, which is the clean limit result for large U.[51]

Results for intermediate disorder are shown in Fig. 4 and the conclusions are the same as for weak disorder: both the UHF and the DFSGW do a good job of reproducing the local charge density, but the UHF fails to reproduce the spin correlations. A closer examination reveals that the UHF value for $\bar{n}_6$ deviates from the exact $\bar{n}_6$ near $U=1.3t$, where local moments form at site 6.

By contrast, results for large disorder in Fig. 5 show that while the DFSGW captures general trends, it does a poor job of reproducing the details of the charge densities and spin correlations as a function of U. Interestingly, the UHF does a remarkably good job of describing both the charge densities and spin correlations for $U \lesssim 6t$. We discuss the large-disorder limit in more detail below, but remark here that the success of UHF can be traced back to the fact that, for $U \ll W$, most sites are empty or doubly occupied, with relatively few having moments. The UHF approximation correctly predicts that spin correlations between isolated moments and their near neighbors vanish when the near-neighbor sites are empty or doubly occupied.

Another measure of the quality of the various approximations is the wave function overlap shown in Figs. 6 and 7. The results of these figures are essentially consistent with the results presented above: the DFSGW has a large overlap with the exact wave function ($|\langle \Psi_{\mathrm{ex}}|\Psi_{\mathrm{GWF}}\rangle| > 0.977$) for weak and intermediate disorders, while for strong disorder the overlap is poor except in the small- and large-U limits. The UHF overlap is generally poor except at small U.

The reason for the difference in the quality of the GWF approximation at intermediate and large disorders is most easily understood by first considering the atomic limit ($t=0$). When $U=0$, the lowest-energy $N_e/2$ sites are doubly occupied while the remaining sites are empty. As U is increased, this arrangement persists until U is larger than the energy difference between the highest-energy doubly occupied site and the lowest-energy empty site, at which point one electron is transferred from the doubly occupied site to the empty site. The process continues as U increases further, with electrons being promoted from doubly occupied sites whenever the cost of double occupancy is greater than the cost of promoting an electron to the next available empty site. The process terminates when $U > W$, at which point all lattice sites are singly occupied. The formation of local moments (singly occupied sites) therefore happens inhomogeneously in the atomic limit.

A nonzero t delocalizes electrons by an amount proportional to t/W and thus makes the charge distribution more homogeneous. Given that the Gutzwiller projection (which is responsible for generating local moments in $|\Psi_{\mathrm{GWF}}\rangle$) is chosen to be spatially uniform, it is unsurprising that the DFSGW approximation should work well for weak disorder ($W \ll D$) and fail for strong disorder ($W \gg D$) where the physics approaches the atomic limit. The surprising result, evident in Fig. 4, is that the moment formation is sufficiently homogeneous at intermediate disorder ($W=D$) to be well represented by our simple variational wave function.

In part, the success of the simple GWF approximation at intermediate disorder can be attributed to the screening of the

disorder potential by interactions (cf. Fig. 1). For small U, correlation effects are minor and the wave function is well represented by the original product state $|\psi_{ps}\rangle$, while for $U>D$ (where correlation effects are important), $\varepsilon_{\min}$ produces a significant renormalization of the impurity potential.

B. Ten-site cluster

We now extend the work of the previous section to consider ten-site clusters with periodic boundary conditions. In this section, we consider results which are averaged over ten randomly generated complexions of the disorder potential. The site potentials are chosen to lie in the interval $(-W/2, W/2)$ and we consider weak $(W/t=4/3)$, intermediate $(W/t=4)$, and strong disorder $(W/t=12)$ cases as before. We show data for $N_e=10$ electrons (half-filling) and $N_e=6$ electrons (near to quarter filling). Given the large Hilbert space (63 500 states for $N_e=10$), we use the Lanczos algorithm to find the exact ground states for comparison to the GWF results.

Results are shown for the DFSGW and PMGW approximations as well as for UHF. Results have not been shown for the PMGW(g,ε) approximation because it was found in Sec. III A to be identical to the PMGW approximation for weak and intermediate disorder and because it is not significantly better than PMGW at large disorder.

Throughout this section, we show error bars for DFSGW results. These error bars give the root-mean-square (rms) variation of $\varepsilon_{\min}$, $g_{\min}$, $\langle \delta E\rangle$, $\langle \delta \bar{n}\rangle$, and $\langle \delta \mathbf{S}\cdot\mathbf{S}'\rangle$ over ten impurity configurations and (for $\langle \delta \bar{n}\rangle$ and $\langle \delta \mathbf{S}\cdot\mathbf{S}'\rangle$) ten sites. The bars are shown for every fourth data point and are of similar size in other GWF approximations. We emphasize that these error bars do not indicate the accuracy of the approximation (the curves themselves indicate this), but describe the site-to-site or sample-to-sample variation in the accuracy of the approximation. Thus, small error bars indicate that the approximation consistently overestimates/underestimates a quantity by the same amount, while large error bars indicate that the quality of the approximation varies significantly from site to site.

1. $N_e=10$ *electrons (half-filling)*

We begin by showing results for the disorder-averaged variational parameters as a function of U at half-filling (Fig. 8). The DFSGW curves are very similar to those shown in Fig. 1 for six sites. As before, differences between the PMGW and DFSGW curves are most pronounced for large disorder and suggest that the PMHF approximation leads to a more complete screening of the disorder potential than does DFSGW.

The variational energies are shown in Fig. 9. For weak and intermediate disorders, the two GWF approximations give nearly identical values for $\langle \delta E\rangle_{\mathrm{GWF}}$. The GWF energies are lower than the UHF energies for small U but larger than the UHF energies at large U. This is consistent with the results for larger clusters in the disorder-free case (cf. Fig. 4 of Ref. 48) and is an indication that the simple GWF is unable to correctly reproduce the Mott transition at large U. For strong disorder, the Mott transition occurs at $U\approx W$ and this sets the energy scale at which the UHF becomes superior to the GWF.

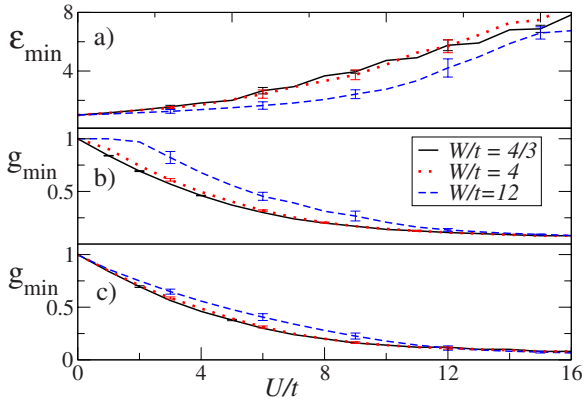

FIG. 8. (Color online) Variational parameters (a) and (b) for the DFSGW and (c) PMGW approximations. Results are shown for ten-site disordered clusters averaged over ten complexions of disorder with $N_e=10$. Data are shown for step size $\Delta U=t$. Error bars give the rms variation of $\varepsilon_{\min}$ and $g_{\min}$ over impurity configurations.

The error in the charge density $\langle \delta \bar{n}\rangle$, defined in Eq. (18), is shown in Fig. 10. At half-filling, the results are largely consistent with those found for six sites. Both the GWF and UHF approximations are good for weak and intermediate disorders, with the DFSGW approximation producing an average error of less than 2.5%; however, all approximations work less well for strong disorder.

The spin correlations, defined in Eq. (18), are shown in Fig. 11 and are also similar to the six-site case. The UHF approximation does a poor job because it generates static local moments, while the GWF approximations work remarkably well for weak and intermediate disorders, having errors of order 1%–2%. For strong disorder, the results are comparable for all approximations, when $U\lesssim 7t$. The GWF approximations are much better than UHF for $U>7$.

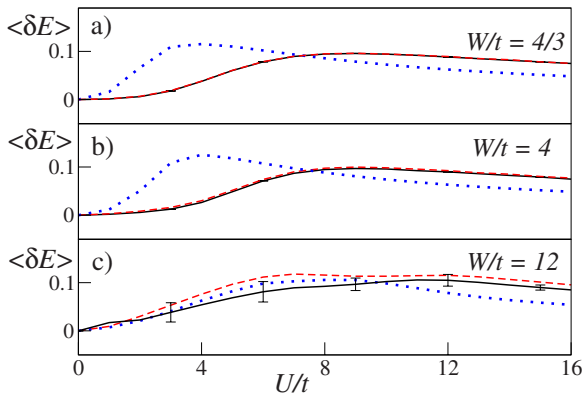

FIG. 9. (Color online) The disorder-averaged energy difference per site between the variational and exact energies for (a) weak, (b) intermediate, and (c) strong disorders at half-filling $(N_e=10)$. The curves are DFSGW (solid black line), PMGW (red dashed line), and UHF (dotted blue line). Data are shown for step size $\Delta U=t$. Error bars give the rms variation of $\langle \delta E\rangle$ over impurity configurations and are too small to see in (a) and (b).

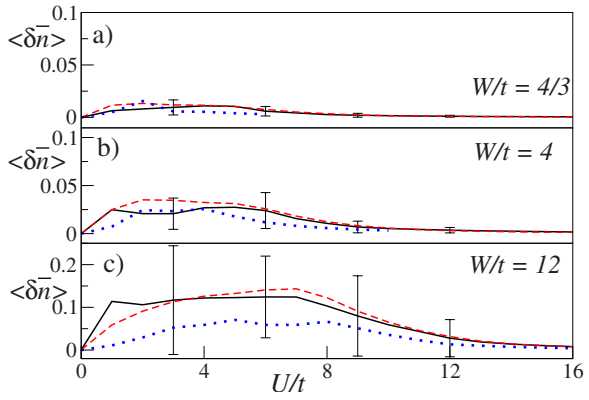

FIG. 10. (Color online) A comparison of the mean absolute difference between the exact and variational local charge densities for the ten-site disordered cluster averaged over ten complexions of disorder with $N_e=10$. Curves are for DFSGW (solid black line), PMGW (red dashed line), and UHF (dotted blue line). Data are shown for step size $\Delta U=t$. Error bars give the rms variation of $\langle \delta\bar{n} \rangle$ over sites and impurity configurations.

2. $N_e=6$ electrons

Away from half-filling, strong correlations play a lesser role than at half-filling and there is no Mott transition. The variational parameters for $N_e=6$ are shown as a function of U in Fig. 12. The most noticeable difference with the half-filled case is that the variational parameters saturate at large U here. The energy scale at which saturation occurs appears to be D for weak and intermediate disorder and W for strong disorder. A consequence of saturation is that the impurity potential is only partially screened at large U. Thus, while the half-filled ground state is the same for ordered and disordered models as $U\rightarrow\infty$, the disorder potential remains relevant at all U's for $N_e=6$. This relevance is illustrated with a simple example: for $W \gg t$ and $U\rightarrow\infty$, the ground state has the N_e sites with the lowest potentials V_i singly occupied and

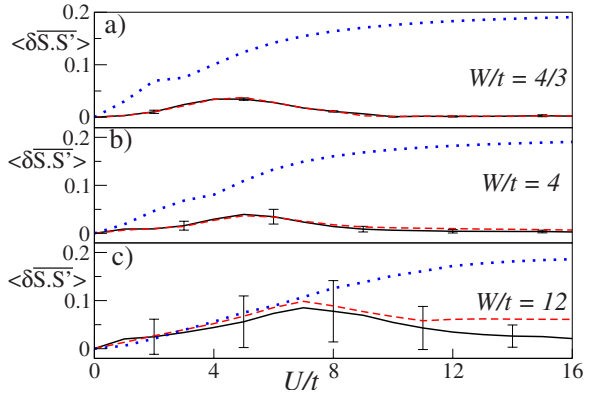

FIG. 11. (Color online) A comparison of the mean absolute difference between the exact and variational expectation values of the near-neighbor spin correlations for the ten-site disordered cluster averaged over ten complexions of disorder, with $N_e=10$. Curves are for DFSGW (solid black line), PMGW (red dashed line), and UHF (dotted blue line). Data are shown for step size $\Delta U=t$. Error bars give the rms variation of $\langle \delta\overline{S\cdot S'} \rangle$ over sites and impurity configurations.

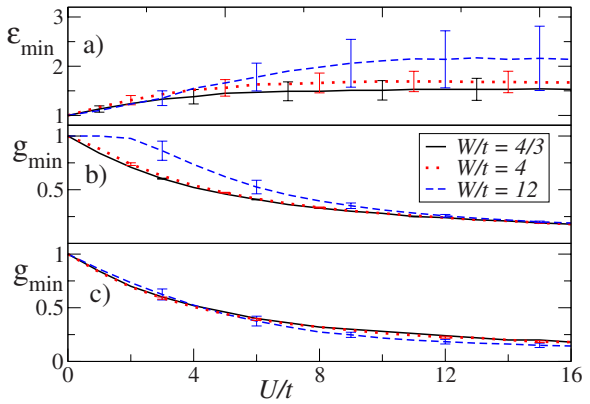

FIG. 12. (Color online) As in Fig. 8, but for $N_e=6$ electrons.

the remaining $N-N_e$ empty. Since there is no Mott transition for $N_e=6$, we expect the GWFs to be valid over a larger range of U than at half-filling. This is supported by Fig. 13, where the GWF energies are generally lower than the UHF energies for weak and intermediate disorders. As before, however, the GWF approximations are worse at large disorder. It is interesting to note that $\langle \delta E \rangle_{\mathrm{GWF}}$ increases roughly linearly with U at large U. Similar behavior was found previously in the ordered case[48] and is consistent with the fact that g_{min} is larger for $N_e=6$ than it is for $N_e=10$ (i.e., the projection of doubly occupied states is less at $N_e=6$ than $N_e=10$).

The charge densities for $N_e=6$ (Fig. 14) are similar to the half-filled case in the sense that the DFSGW charge densities are comparable to UHF (Ref. 20) at weak and intermediate disorders, but are less accurate than UHF at strong disorder. Similarly to the $N_e=10$ case, the *average* spin correlations (Fig. 15) are reasonably well reproduced at weak and intermediate disorder.

IV. DISCUSSION

The GWFs used in this work make two key simplifying assumptions: first, that the correlation physics is approximately local and can be represented by a Gutzwiller partially projected wave function and second, that the spatial inhomogeneity associated with the disorder potential can be incor-

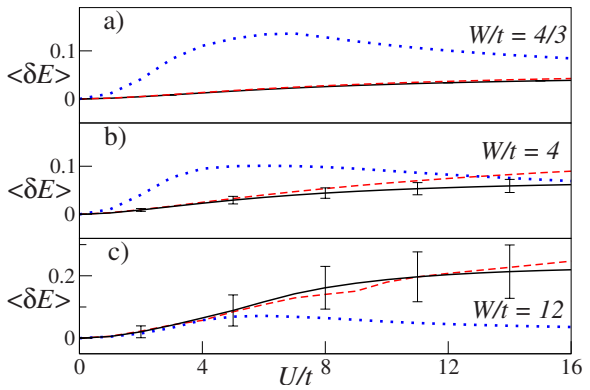

FIG. 13. (Color online) As in Fig. 9, but for $N_e=6$ electrons.

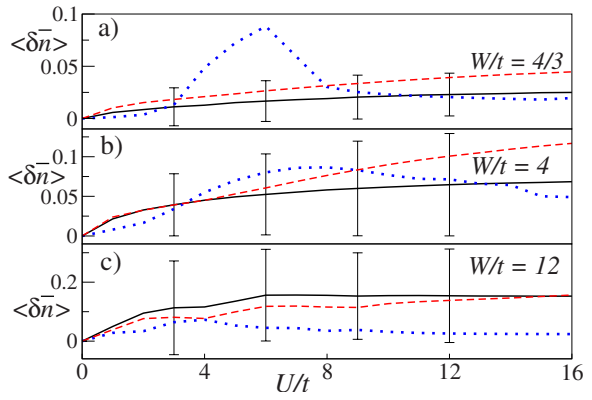

FIG. 14. (Color online) As in Fig. 10, but for $N_e=6$ electrons. Error bars are larger here than for $N_e=10$ because of the larger site-to-site variations in the accuracy of the GWF.

porated entirely within the uncorrelated product state. In this section, we discuss these two assumptions, keeping in mind that, while it is possible to treat a large number of variational parameters using statistical sampling methods,[35] many of the interesting questions relating to disordered systems require the ability to study large system sizes, and that it is therefore desirable to restrict the number of variational parameters as much as possible. The results shown in this paper give some clues as to how this can be done.

There are two distinct regimes in our calculations, distinguished by the strength of the *screened* disorder potential, which in the DFSGW is $W'=W/\varepsilon_{\min}$. For $W\lesssim D$, W' is sufficiently small that the GWFs used in this work give similar results for $\langle\delta E\rangle$ as existing calculations for the ordered case (i.e., Fig. 4 of Ref. 48). In Ref. 48, it was shown that the simplest GWF could be improved by inclusion of a long-range Jastrow factor and the similarity of our results to theirs has a similar implication. Interestingly, there is nothing in our results to suggest that adopting spatially inhomogeneous variational parameters would make a significant improvement. (Recall, Figs. 3 and 4, the accuracy with which the DFSGW approximation reproduces the *local* charge density and spin correlations.) It appears as if, for $W\lesssim D$, spatial inhomogeneity can be adequately incorporated in the product state provided that screening is included, either through a Hartree-Fock determination of the product state or through a

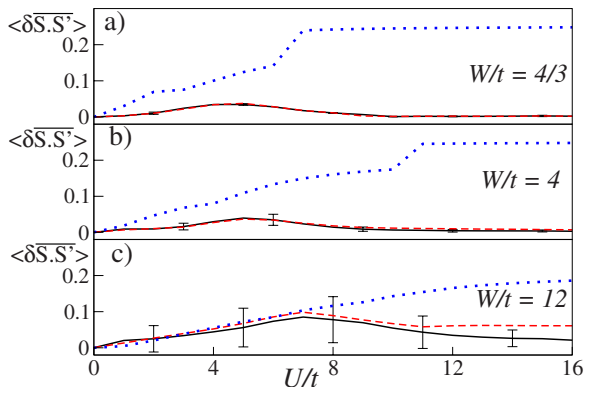

FIG. 15. (Color online) As in Fig. 11, but for $N_e=6$ electrons.

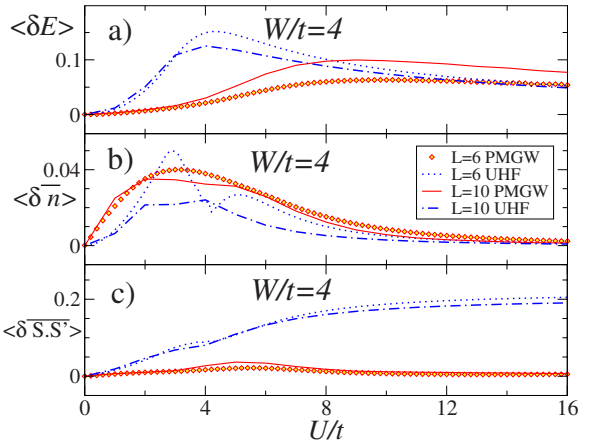

FIG. 16. (Color online) A comparison of the mean absolute difference between the exact and the variational (a) energies, (b) local charge densities, and (c) near-neighbor spin correlations. The results are shown for ten-site clusters averaged over ten complexions of disorder (red solid lines for PMGW and blue dot-dashed lines for UHF) and six-site clusters averaged over 15 configurations of disorder (diamonds for PMGW and blue dotted lines for UHF). Data are shown for step size $\Delta U=t$ for ten-site clusters and $\Delta U=0.1t$ for six-site clusters.

variational parameter. This represents a huge savings of computational effort since, if one makes a physically reasonable ansatz for the form of the Jastrow factor, the number of variational parameters can be reduced to four: a screening parameter ε, a projection parameter g, and a pair of parameters for the Jastrow factor.[35,48]

For strong disorder, the situation is different since spatial fluctuations of the charge density are significant. It appears that, in this case, spatial inhomogeneity cannot be included solely in $|\Psi_{\rm ps}\rangle$ but must be included in the variational parameters as well. This was the approach taken in Ref. 35 where the local variational parameters g and ε were allowed to vary from site to site (but the nonlocal Jastrow factors were treated as spatially homogeneous in order to reduce the computational workload) on lattices of $N\sim 100$ sites. It is unclear that any simplification of this approach is possible in the large-disorder limit.

Finally, we comment on finite-size effects. We compare $\langle\delta E\rangle$, $\langle\delta\bar{n}\rangle$, and $\langle\delta\mathbf{S}\cdot\mathbf{S}'\rangle$, for six and ten site clusters at half-filling and intermediate disorder in Fig. 16. The GWF energy differences increase with system size and, in the weak disorder case, appear to scale toward the clean limit results shown in Fig. 4 of Ref. 48 for large systems. We note that, while there are quantitative differences, $\langle\delta E\rangle$ for the ten-site clusters has the same qualitative U dependence as for the larger clean limit systems. More importantly for this work, $\langle\delta\bar{n}\rangle$ and $\langle\delta\mathbf{S}\cdot\mathbf{S}'\rangle$ are nearly independent of system size. This is consistent with earlier scaling results in the disorder-free case[51] and suggests that the high accuracy of the results in Figs. 16(b) and 16(c) will extend to larger systems. Thus, ability to benchmark GWF trial functions is not inhibited by finite-size effects.

V. CONCLUSIONS

We have studied the Anderson-Hubbard model, one of the simplest model Hamiltonians that can describe correlated

electrons moving on a disordered lattice. We have compared the exact and variational ground states for disordered one-dimensional chains up to a length of ten sites. The main focus of our calculations was on finding the simplest variational states that accurately include the effects of disorder. The quality of the approximations was determined by comparing a number of physical quantities—the ground-state energy, local charge densities, and near-neighbor spin correlations—to the exact results. Because it has been, until recently, the standard tool for studying disordered systems, we also compared our variational states to the unrestricted Hartree-Fock approximation.

Our main conclusion is that, for weak and intermediate disorder, an accurate description of the ground state can be obtained by taking a spatially inhomogeneous product state and spatially homogeneous variational parameters. This represents a significant reduction in computational workload over the more general case where both the product state and variational parameters must be inhomogeneous.

ACKNOWLEDGMENTS

This work was supported in part by the NSERC.

APPENDIX: TWO-SITE CLUSTER

We compare the different product states for a two-site system, where an analytical solution can be found. For this cluster we choose the on-site energy of sites one and two to be V and 0, respectively, and take $N_e=2$ (corresponding to half-filling). Then

$$|\psi_{\mathrm{ps}}\rangle = \frac{1}{\sqrt{N_\uparrow N_\downarrow}}(c_{1\uparrow}^\dagger + a_\uparrow c_{2\uparrow}^\dagger)(c_{1\downarrow}^\dagger + a_\downarrow c_{2\downarrow}^\dagger)|0\rangle$$
$$= \frac{1}{\sqrt{1+a_\uparrow^2+a_\downarrow^2+(a_\uparrow a_\downarrow)^2}}(|\uparrow\downarrow\rangle|0\rangle - a_\uparrow|\downarrow\rangle|\uparrow\rangle + a_\downarrow|\uparrow\rangle|\downarrow\rangle + a_\uparrow a_\downarrow|0\rangle|\uparrow\downarrow\rangle), \quad \text{(A1)}$$

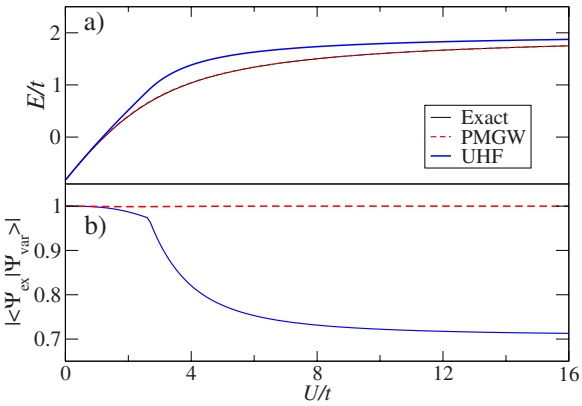

FIG. 17. (Color online) Variational solutions for the two-site Anderson-Hubbard model with $V=2.0t$. (a) A comparison of the PMGW variational energy with the exact and UHF ground-state energies. The exact energies coincide with the PMGW energies. (b) The wave function overlap $|\langle\Psi_{\mathrm{ex}}|\Psi_{\mathrm{var}}\rangle|$.

where $N_\sigma^{-1/2}\binom{1}{a_\sigma}$ are normalized eigenvectors of the matrix form of $\mathcal{H}_{\mathrm{bl}}$ for spin σ,

$$H_{\mathrm{bl},\sigma} = \begin{pmatrix} V' + U\bar{n}_{1-\sigma} & -t \\ -t & U\bar{n}_{2-\sigma}, \end{pmatrix}, \quad \text{(A2)}$$

with $V'=V/\varepsilon$,

$$a_\sigma = \frac{1}{2t}\{V' + U(\bar{n}_{1-\sigma} - \bar{n}_{2-\sigma}) + \sqrt{[U(\bar{n}_{1-\sigma} - \bar{n}_{2-\sigma}) + V']^2 + 4t^2}\}, \quad \text{(A3)}$$

and the many-particle states are defined as $|\uparrow\downarrow\rangle|0\rangle = c_{1\uparrow}^\dagger c_{1\downarrow}^\dagger|0\rangle$, $|\uparrow\rangle|\downarrow\rangle = c_{1\uparrow}^\dagger c_{2\downarrow}^\dagger|0\rangle$, etc.

Using Eqs. (2) and (A1), $|\Psi_{\mathrm{GWF}}\rangle$ is written as

$$|\Psi_{\mathrm{GWF}}\rangle = \frac{1}{\sqrt{1+a_\uparrow^2+a_\downarrow^2+(a_\uparrow a_\downarrow)^2}}(g|\uparrow\downarrow\rangle|0\rangle - a_\uparrow|\downarrow\rangle|\uparrow\rangle + a_\downarrow|\uparrow\rangle \times|\downarrow\rangle + g a_\uparrow a_\downarrow|0\rangle|\uparrow\downarrow\rangle), \quad \text{(A4)}$$

and

$$E_{\mathrm{GWF}} = \frac{g^2[(1+a_\uparrow^2 a_\downarrow^2)U + 2V] - 2tg(a_\uparrow + a_\downarrow)(a_\uparrow a_\downarrow + 1) + V(a_\uparrow^2 + a_\downarrow^2)}{g^2[1+(a_\uparrow a_\downarrow)^2] + a_\uparrow^2 + a_\downarrow^2}. \quad \text{(A5)}$$

Numerical results for this cluster show that the DFSGW, PMGW (g,ε), and PMGW energies are the same, and we therefore only show the results for PMGW in Fig. 17. In this figure, we compare the magnitude of the PMGW energies with the UHF and exact energies. We also compare the overlaps of the PMGW and UHF wave functions with the exact wave functions. The overlaps are defined as $|\langle\Psi_{\mathrm{ex}}|\Psi_{\mathrm{var}}\rangle|$, where $\langle\Psi_{\mathrm{ex}}|$ is the complex conjugate of the exact ground-state eigenvector of $\mathcal{H}$. The reason to study both ground-state energies and overlaps is that a lower variational energy does not necessarily imply a better variational wave function.

In general, UHF energies are lower than PMHF energies (not shown) suggesting that the UHF approximation is better than the PMHF one. However, after the projection the situa-

tion is reversed. In Fig. 17 one sees that PMGW energies are exact and that the UHF energies are higher than the PMGW energies for $U/t>2$, where magnetic moments develop in the UHF states. Similarly, $|\langle\Psi_{ex}|\Psi_{PMGW}\rangle|=1$ while $|\langle\Psi_{ex}|\Psi_{UHF}\rangle|$ decreases rapidly as moments develop. This is consistent with the ordered case,[48] where the GWF is exact for the two-site problem but is approximate for larger system sizes.

*avid@physics.queensu.ca

[1] B. L. Altshuler and A. G. Aronov, in *Electron-Electron Interactions in Disordered Systems*, Modern Problems in Condensed Matter Sciences Vol. 10, edited by A. L. Efros and M. Pollak (North-Holland, New York, 1985).

[2] M. Imada, A. Fujimori, and Y. Tokura, Rev. Mod. Phys. **70**, 1039 (1998).

[3] H. Alloul, J. Bobroff, M. Gabay, and P. J. Hirschfeld, Rev. Mod. Phys. **81**, 45 (2009).

[4] Y. Ando, A. N. Lavrov, and S. Komiya, Phys. Rev. Lett. **90**, 247003 (2003).

[5] K. Fujita, T. Noda, K. M. Kojima, H. Eisaki, and S. Uchida, Phys. Rev. Lett. **95**, 097006 (2005).

[6] R. J. Gooding, N. M. Salem, R. J. Birgeneau, and F. C. Chou, Phys. Rev. B **55**, 6360 (1997).

[7] M. Hashimoto, T. Yoshida, A. Fujimori, D. H. Lu, Z.-X. Shen, M. Kubota, K. Ono, M. Ishikado, K. Fujita, and S. Uchida, Phys. Rev. B **79**, 144517 (2009).

[8] M. A. Kastner, R. J. Birgeneau, G. Shirane, and Y. Endoh, Rev. Mod. Phys. **70**, 897 (1998).

[9] E. Lai and R. J. Gooding, Phys. Rev. B **57**, 1498 (1998).

[10] A. Sugimoto, S. Kashiwaya, H. Eisaki, H. Kashiwaya, H. Tsuchiura, Y. Tanaka, K. Fujita, and S. Uchida, Phys. Rev. B **74**, 094503 (2006).

[11] A. D. Caviglia, S. Gariglio, N. Reyren, D. Jaccard, T. Schneider, M. Gabay, S. Thiel, G. Hammerl, J. Mannhart, and J. –M. Triscone, arXiv:0807.0585 (unpublished).

[12] A. Ohtomo and H. Y. Hwang, Nature (London) **427**, 423 (2004).

[13] N. Reyren, S. Thiel, A. D. Caviglia, L. Fitting Kourkoutis, G. Hammerl, C. Richter, C. W. Schneider, T. Kopp, A.-S. Rüetschi, D. Jaccard, M. Gabay, D. A. Muller, J.-M. Triscone, and J. Mannhart, Science **317**, 1196 (2007).

[14] K. Ueno, S. Nakamura, H. Shimotani, A. Ohtomo, N. Kimura, T. Nojima, H. Aoki, Y. Iwasa, and M. Kawasaki, Nature Mater. **7**, 855 (2008).

[15] T. Schneider A. D. Caviglia, S. Gariglio, N. Reyren, D. Jaccard, and J. –M. Triscone, arXiv:cond-mat/0807.0774 (unpublished).

[16] S. V. Kravchenko and M. P. Sarachik, Rep. Prog. Phys. **67**, 1 (2004).

[17] J. Hubbard, Proc. R. Soc. London, Ser. A **276**, 238 (1963).

[18] A. Georges, G. Kotliar, W. Krauth, and M. Rozenberg, Rev. Mod. Phys. **68**, 13 (1996).

[19] M. Milovanovic, S. Sachdev, and R. N. Bhatt, Phys. Rev. Lett. **63**, 82 (1989).

[20] X. Chen, A. Farhoodfar, T. McIntosh, R. J. Gooding, and P. Leung, J. Phys.: Condens. Matter **20**, 345211 (2008).

[21] F. Fazileh, R. J. Gooding, W. A. Atkinson, and D. C. Johnston, Phys. Rev. Lett. **96**, 046410 (2006).

[22] D. Heidarian and N. Trivedi, Phys. Rev. Lett. **93**, 126401 (2004).

[23] M. A. Tusch and D. E. Logan, Phys. Rev. B **48**, 14843 (1993).

[24] E. C. Andrade, E. Miranda, and V. Dobrosavljevic, arXiv:0811.0320 (unpublished).

[25] M. Balzer and M. Potthoff, Physica B (Amsterdam) **359-361**, 768 (2005).

[26] K. Byczuk, W. Hofstetter, and D. Vollhardt, Phys. Rev. Lett. **94**, 056404 (2005).

[27] V. Dobrosavljević, A. A. Pastor, and B. K. Nikolić, Europhys. Lett. **62**, 76 (2003).

[28] M. S. Laad, L. Craco, and E. Müller-Hartmann, Phys. Rev. B **64**, 195114 (2001).

[29] P. Lombardo, R. Hayn, and G. I. Japaridze, Phys. Rev. B **74**, 085116 (2006).

[30] Y. Song, R. Wortis, and W. A. Atkinson, Phys. Rev. B **77**, 054202 (2008).

[31] M. Ulmke, V. Janis, and D. Vollhardt, Phys. Rev. B **51**, 10411 (1995).

[32] S. Chiesa, P. B. Chakraborty, W. E. Pickett, and R. T. Scalettar, Phys. Rev. Lett. **101**, 086401 (2008).

[33] R. Kotlyar and S. Das Sarma, Phys. Rev. Lett. **86**, 2388 (2001).

[34] B. Srinivasan, G. Benenti, and D. L. Shepelyansky, Phys. Rev. B **67**, 205112 (2003).

[35] M. E. Pezzoli, F. Becca, M. Fabrizio, and G. Santoro, Phys. Rev. B **79**, 033111 (2009).

[36] M. C. Gutzwiller, Phys. Rev. **134**, A923 (1964).

[37] M. C. Gutzwiller, Phys. Rev. **137**, A1726 (1965).

[38] H. Yokoyama and H. Shiba, J. Phys. Soc. Jpn. **56**, 1490 (1987).

[39] F. Gebhard and D. Vollhardt, Phys. Rev. Lett. **59**, 1472 (1987).

[40] F. Gebhard and D. Vollhardt, Phys. Rev. B **38**, 6911 (1988).

[41] W. Metzner and D. Vollhardt, Phys. Rev. Lett. **59**, 121 (1987).

[42] W. Metzner and D. Vollhardt, Phys. Rev. B **37**, 7382 (1988).

[43] W. Metzner and D. Vollhardt, Phys. Rev. Lett. **62**, 324 (1989).

[44] D. Ceperley, G. V. Chester, and M. H. Kalos, Phys. Rev. B **16**, 3081 (1977).

[45] E. Koch, O. Gunnarsson, and R. M. Martin, Phys. Rev. B **59**, 15632 (1999).

[46] H. Yokoyama and H. Shiba, J. Phys. Soc. Jpn. **56**, 3582 (1987).

[47] M. Capello, F. Becca, M. Fabrizio, S. Sorella, and E. Tosatti, Phys. Rev. Lett. **94**, 026406 (2005).

[48] H. Yokoyama and H. Shiba, J. Phys. Soc. Jpn. **59**, 3669 (1990).

[49] S. Sorella, Phys. Rev. B **71**, 241103(R) (2005).

[50] Note that the most general decomposition includes spin-flip fields due to tilted moments. These fields have been shown to be important for some spin-glass phases but are not relevant to the paramagnetic approximations used here. See Ref. 20 for a complete discussion.

[51] T. A. Kaplan, P. Horsch, and P. Fulde, Phys. Rev. Lett. **49**, 889 (1982).